

# THROUGH-THE-WALL RADAR IMAGING BASED ON MODIFIED BAYESIAN COMPRESSIVE SENSING

*Qisong Wu, Yimin D. Zhang, Moeness G. Amin, and Fauzia Ahmad*

Center for Advanced Communications, Villanova University, Villanova, PA 19085, USA

## ABSTRACT

In this paper, a novel modified complex multi-task Bayesian compressive sensing (MCMT-BCS) algorithm is proposed to acquire high-resolution images in stepped-frequency through-the-wall radar imaging (TWRI) exploiting multipath. Unlike traditional TWRI approaches that assume frequency-independent scattering model, we develop a practical subband scattering model to characterize real-world scattering mechanisms. The target imaging is reformulated as a multi-task sparse signal recovery problem across all frequency subbands as well as multipath modes, where the sparse entries of each task share the same support in the imaged scene. The proposed MCMT-BCS algorithm accounts for both types of coexisting group sparsity to achieve improved high-resolution imaging capability. Simulation results verify the effectiveness of the proposed algorithm.

**Index Terms**— Through-the-wall radar imaging, sparse construction, multipath exploitation, Bayesian compressive sensing, group sparsity.

## 1. INTRODUCTION

Imaging through building walls using radar has received significant attention due to its numerous civil and military applications. Through-the-wall radar imaging (TWRI) has the capability of acquiring high-resolution images of targets of interest behind an opaque obstacle [1–5].

To acquire high-resolution images, TWRI systems have to utilize wide-band signals. A stepped-frequency wide-band signal is a good choice for low-cost implementation [4]. A number of TWRI algorithms have been developed to acquire high-resolution images [6–10]. However, all these algorithms are developed based on the assumption that the scattering coefficients are independent of the transmitting frequencies. Considering the fact that the transmitted signal bandwidth typically ranges from hundreds of Megahertz to a few Gigahertz [4, 6, 7], such frequency-independent scattering model is impractical according to the radar cross section (RCS) principle [1]. On the other hand, there exist multipath propagations that stem from electromagnetic wave reflections off the targets in conjunction with the walls. Such multipath reflections may lead to the so-called ghost targets at positions away from those of the actual targets. These ghost targets clutter the imaged scene and make target detection difficult [9]. Earlier work proposed an effective approach to mitigate the effects of multipath propagation [1], whereas more recent approaches are based on multipath exploitation for target

signal enhancement [9, 10]. Compressed observations arise primarily due to logistic difficulties in securing observations at desired antenna positions and frequency bins. In this aspect, multipath exploitation has been effectively implemented using compressive sensing techniques that take advantages of the group sparsity of the targets due to multipath propagations. In essence, the multipath scenes assume the same target support but differ in target scattering coefficients [10].

A number of algorithms have been developed to recover group sparse signals. These algorithms include greedy-based algorithms, such as block orthogonal matching pursuit (BOMP) [11], and basis pursuit-based ones, such as group basis pursuit (GBP) [12] and group Lasso (gLasso) [13]. Group sparse Bayesian learning algorithms based on relevance vector machine (RVM) form a different class of sparse signal reconstruction algorithms, which generally yield improved performance over other techniques particularly in the presence of high-coherence sensing vectors [14, 15]. The multi-task compressive sensing (mt-CS) algorithm [15] provides solutions to a large class of group sparse problems. This approach is extended to effectively process complex-valued problems as encountered in radar sensing applications [16]. However, those algorithms can be used to recover sparse signals with group structure across tasks, and take no consideration of the group sparsity in each task.

In this paper, a modified complex multi-task Bayesian compressive sensing (MCMT-BCS) algorithm is proposed to acquire high-resolution images by exploiting both types of group sparsity due to multipath propagations and frequency-dependent scattering characteristics. The latter is represented using a subband scattering model where the target scattering coefficients are assumed to be constant within a subband but vary independently across different subbands. The TWRI approach is then formulated as a multi-task sparse signal recovery problem, and the proposed MCMT-BCS algorithm accounts for both types of coexisting group sparsity to achieve improved high-resolution imaging capability. The superiority of the proposed algorithm over existing techniques is demonstrated by simulation results.

**Notations:** We use lower-case (upper-case) bold characters to denote vectors (matrices). In particular,  $\mathbf{I}_N$  denotes the  $N \times N$  identity matrix.  $(\cdot)^T$  denotes the transpose of a matrix or vector,  $p(\cdot)$  denotes the probability density function (pdf),  $\mathcal{N}(x|a, b)$  denotes that random variable  $x$  follows a Gaussian distribution with mean  $a$  and variance  $b$ ,  $\lceil x/y \rceil$  denotes the modulus after  $x$  over  $y$ , and  $\lfloor x/y \rfloor$  denotes the remainder after  $x$  over  $y$ . In addition,  $\text{Tr}(\cdot)$  denotes the trace operation of a

matrix,  $\text{Re}(\cdot)$  and  $\text{Im}(\cdot)$ , respectively, represent the real and imaginary components of a complex element.

## 2. SIGNAL MODEL

The signal model is formulated using a monostatic stepped-frequency approach [4]. Assume that  $N$  wideband transceivers are arranged as a uniform linear array (ULA) with element positions  $x_n, n = 1, \dots, N$ , that are uniformly separated by an inter-element spacing of  $d$ . In the stepped-frequency approach, a wideband pulse is approximated by  $M$  monochromatic signals. The frequency  $f_m$  with  $m \in \{1, \dots, M\}$  are uniformly spaced over the signal bandwidth  $B$ . In the case of compressed observations, the transceivers and employed frequencies can be both nonuniform, describing random spatial-frequency sampling. In this paper, only target returns are considered after the front-wall responses are properly suppressed using one of the wall clutter mitigation techniques [17–19]. In the monostatic operation, the target returns can be expressed as [10],

$$y(m, n) = \sum_{p=1}^{N_x N_y} w_p \exp(-j2\pi f_m \tau_{pn}), \quad (1)$$

where  $N_x$  and  $N_y$ , respectively, denote the number of gates in crossrange and downrange within the region of interest,  $\tau_{pn}$  represents the round-trip propagation delay between the  $p$ th scatterer and  $n$ th transceivers, and  $w_p$  is the complex reflectivity corresponding to the  $p$ th pixel. We assume the knowledge or an accurate estimation of the wall thickness and permittivity and thus the wall effect can be perfectly compensated [1, 2].

### 2.1. Subband scattering model

To model frequency-dependent scattering coefficients, we group the  $M$  measured stepped-frequencies into  $L$  subbands. These frequencies,  $\{f_m, m = 1, \dots, M\}$ , are labelled as  $\{f_1^{(1)}, \dots, f_{g_1}^{(1)}, \dots, f_{g_L}^{(L)}\}$ , where  $g_l$  is the number of frequencies in the  $l$ th subband, and  $\sum_{l=1}^L g_l = M$ . As such, Eq. (1) can be rewritten in each subband as,

$$y^{(l)}(m', n) = \sum_{p=1}^{N_x N_y} w_p^{(l)} \exp(-j2\pi f_{m'}^{(l)} \tau_{pn}), \quad (2)$$

where  $m' \in \{1, \dots, g_l\}$ , and  $w_p^{(l)}$  is frequency-dependent scattering coefficient of the  $p$ th pixel at the  $l$ th subband. Stacking the measurements  $y^{(l)}(m', n)$  corresponding to the frequencies belonging to the  $l$ th subband, we have

$$\mathbf{y}^{(l)} = \mathbf{\Phi}^{(l)} \mathbf{w}^{(l)}, \quad (3)$$

where  $\mathbf{y}^{(l)} = [y^{(l)}(1, 1), \dots, y^{(l)}(1, N), \dots, y^{(l)}(g_l, N)]^T \in \mathcal{C}^{g_l N}$ ,  $\mathbf{\Phi}^{(l)} \in \mathcal{C}^{g_l N \times N_x N_y}$  whose  $(i, p)$ th element is given by

$$[\mathbf{\Phi}^{(l)}]_{ip} = \exp(-j2\pi f_{m'}^{(l)} \tau_{pn}), \quad (4)$$

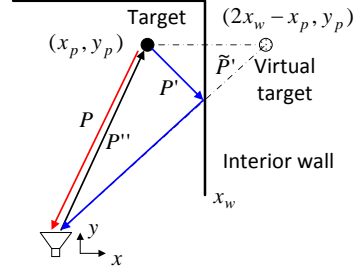


Fig. 1. Multipath propagations via reflections at interior walls

for  $i \in \{1, \dots, g_l N\}$ ,  $m = \lceil i/g_l \rceil$ , and  $n = \lfloor i/g_l \rfloor$ , and  $\mathbf{w}^{(l)} \in \mathcal{C}^{N_x N_y}$ . Note that the supports of the sparse targets are identical across the  $L$  groups (i.e., the nonzero entries of  $\mathbf{w}^{(l)}$  lie in the same positions across different values of  $l$ ), whereas their scattering coefficients are generally different.

### 2.2. Interior Wall Multipath

In TWRI, multipath propagation corresponds to indirect paths which involve secondary reflections at an interior wall. The dominant multipath component corresponds to a ‘bistatic’ scattering scenario. That is, the transmitted signal propagates directly to the scatterer and then the scattered wave travels back to the transceiver after being reflected by an interior wall or vice versa. This type of multipath leads to ghost targets that lie within the perimeter of the imaged room [9, 10]. Other multipath scenarios exist, but can usually be mitigated by time-gating due to weak ghost targets or because they are located outside the room.

For example, consider the effect of the interior specular wall located at  $x = x_w$  in Fig. 1. The effect of the front wall is ignored for simplicity. The  $p$ th target is located at  $\mathbf{z}_p = [x_p, y_p]^T$ . The direct path is from a transceiver to the target along the path  $P''$  and back to the receiver along the path  $P$ , whereas the dominant multipath propagation consists of the forward path from the transceiver to the target along the path  $P''$  and the return path from the target via a reflection at the interior wall along path  $P'$ . In this case, the length of the return path  $P'$  can be equivalently computed as the distance between the transceiver and the virtual target located at  $\mathbf{z}'_p = [2x_w - x_p, y_p]$ . A similar multipath consists of propagation along  $P'$  and  $P''$  in the reverse direction. We can calculate the multipaths via other interior walls in a similar manner. Assume one direct path and a maximum number of  $K - 1$  multipaths. Then, the forward model with multipath propagations in the  $l$ th subband can be modified as [10],

$$\tilde{\mathbf{y}}^{(l)} = \mathbf{\Phi}_1^{(l)} \mathbf{w}_1^{(l)} + \mathbf{\Phi}_2^{(l)} \mathbf{w}_2^{(l)} + \dots + \mathbf{\Phi}_K^{(l)} \mathbf{w}_K^{(l)}, \quad (5)$$

where  $\mathbf{\Phi}_1^{(l)} \in \mathcal{C}^{g_l N \times N_x N_y}$  and  $\mathbf{w}_1^{(l)} \in \mathcal{C}^{N_x N_y}$  respectively denote the measurement matrix and complex reflectivities in the direct path, whereas  $\mathbf{\Phi}_k^{(l)}$  and  $\mathbf{w}_k^{(l)}$  with  $k \in \{2, \dots, K\}$  are those corresponding to the  $k$ th multipath. It should be noted that the complex reflectivities  $\mathbf{w}_k^{(l)}, k = 1, \dots, K$  shares the same sparsity support across all paths, i.e., they have the same respective positions of nonzero entries, although the exact value of the reflectivity coefficients generally differ. This

group sparse property provides a feasible way to enhance the recovery of scatterers.

Rewrite Eq. (5) as

$$\tilde{\mathbf{y}}^{(l)} = \mathbf{\Psi}^{(l)} \tilde{\mathbf{w}}^{(l)} + \boldsymbol{\epsilon}^{(l)}, \quad l \in \{1, \dots, L\}, \quad (6)$$

$$\tilde{\mathbf{w}}^{(l)} = [\mathbf{w}_1^{(l)}, \dots, \mathbf{w}_K^{(l)}]^T \in \mathcal{C}^{N_x N_y K}, \quad (7)$$

$$\mathbf{w}_k^{(l)} = [w_{1,k}^{(l)}, \dots, w_{N_x N_y, k}^{(l)}] \in \mathcal{C}^{1 \times N_x N_y}, \quad (8)$$

where  $\tilde{\mathbf{y}}^{(l)} \in \mathcal{C}^{g_l N}$  denotes observation data in the  $l$ th subband,  $\mathbf{\Psi}^{(l)} = [\mathbf{\Psi}_1^{(l)}, \dots, \mathbf{\Psi}_K^{(l)}] \in \mathcal{C}^{g_l N \times N_x N_y K}$  is the joint measurement matrix in the  $l$ th subband,  $\tilde{\mathbf{w}}^{(l)}$  represents the complex reflectivity vector. Without loss of generality, a measurement noise vector  $\boldsymbol{\epsilon}^{(l)} \in \mathcal{C}^{g_l N}$  is added in (6).

It becomes evident that two types of group sparsity, respectively due to multipath propagation and subband observations, coexist in this TWRI problem. That is,  $\mathbf{w}_k^{(l)}$  in Eq. (8) with  $k \in (1, \dots, K)$  shares the same support across all paths for  $k = 1, \dots, K$  in each subband, and  $\tilde{\mathbf{w}}^{(l)}$  in Eq. (7) shares the same support across subbands for  $l = 1, \dots, L$ . It is noted, however, that the measurement signals are resolvable for each subband but generally unresolvable for the multipaths.

### 3. MODIFIED COMPLEX MULTI-TASK BAYESIAN COMPRESSIVE SENSING

Conventional group inversion algorithms, such as BOMP [11] and gLasso [13], guarantee reliable estimations only when the dictionary meets the so-called G-RIP condition [20]. Unfortunately, such a condition cannot be easily verified since it is computationally demanding [21]. The G-RIP condition requires that the dictionary behaves like an isometry system on sparse signal. For high-resolution TWRI, however, the coherence of the dictionary  $\mathbf{\Phi}$  may become very high. In this case, sparse Bayesian learning algorithms based on RVM generally yield improved performance [14, 15]. The work in [16] proposed an effective approach to complex group sparse signal recovery based on the Bayesian learning technique under a multi-task model. However, this approach only considers the group structure across tasks and takes no consideration of the group sparsity in each task. The objective of this paper is to develop a modified complex multi-task Bayesian compressive sensing (MCMT-BCS) algorithm to handle the aforementioned TRWI problem wherein two types of group sparsity coexist.

Similar to the work in [16], we place a Gaussian distribution on the target reflectivities and the real and imaginary components follow an independent Gaussian distribution with mean zero and pixel-dependent variance  $\alpha_m$ , i.e.,

$$w_{p,k}^{(IR)} \sim \mathcal{N}(w_{p,k}^{(IR)} | 0, \alpha_p), \quad w_{p,k}^{(II)} \sim \mathcal{N}(w_{p,k}^{(II)} | 0, \alpha_p), \quad (9)$$

where  $p \in (1, \dots, N_x N_y)$ ,  $k \in (1, \dots, K)$ ,  $w_{p,k}^{(IR)}$  and  $w_{p,k}^{(II)}$  are respectively the real and imaginary parts of the  $p$ -th complex scattering coefficient of the  $k$ th path in the  $l$ th subband. It is emphasized that, because  $\alpha_p$ , to be determined later, varies with each pixel, the overall distribution of the

reflection coefficients does not assume a specific distribution across the scene.

It is important to note that the parameters  $\boldsymbol{\alpha} = \{\alpha_p\}_{p=1, N_x N_y}$  assume identical values across the  $K$  paths and the  $L$  subbands. The MCMT-BCS algorithm extends the approach in [16] to group sparsity across both  $L$  subbands and  $K$  paths by shared parameters  $\alpha_p$ . The benefits of this approach will be demonstrated later through simulations.

Without loss of generality, a Gaussian prior is placed on the additive measurement noise, i.e.,

$$\hat{\boldsymbol{\epsilon}}_{m,k}^{(IR)} \sim \mathcal{N}(\hat{\boldsymbol{\epsilon}}_{m,k}^{(IR)} | 0, \beta_0), \quad \hat{\boldsymbol{\epsilon}}_{m,k}^{(II)} \sim \mathcal{N}(\hat{\boldsymbol{\epsilon}}_{m,k}^{(II)} | 0, \beta_0), \quad (10)$$

where  $\hat{\boldsymbol{\epsilon}}_{m,k}^{(IR)}$  and  $\hat{\boldsymbol{\epsilon}}_{m,k}^{(II)}$  are the real and imaginary parts of the complex noise respectively, and  $\beta_0$  is the noise variance. Now we consider the posterior pdf of

$$\hat{\boldsymbol{\omega}}^{(l)} = [w_{1,1}^{(IR)}, \dots, w_{N_x N_y, K}^{(IR)}, w_{1,1}^{(II)}, \dots, w_{N_x N_y, K}^{(II)}]. \quad (11)$$

The posterior distribution of  $\hat{\boldsymbol{\omega}}^{(l)}$  is evaluated analytically based on Bayes' rule as,

$$\Pr(\hat{\boldsymbol{\omega}}^{(l)} | \hat{\mathbf{y}}^{(l)}, \mathbf{\Psi}^{(l)}, \boldsymbol{\alpha}, \beta_0) = \mathcal{N}(\hat{\boldsymbol{\omega}}^{(l)} | \boldsymbol{\mu}^{(l)}, \boldsymbol{\Sigma}^{(l)}), \quad (12)$$

where

$$\boldsymbol{\mu}^{(l)} = \beta_0^{-1} \boldsymbol{\Sigma}^{(l)} (\hat{\mathbf{\Psi}}^{(l)})^T \hat{\mathbf{y}}^{(l)}, \quad (13)$$

$$\boldsymbol{\Sigma}^{(l)} = \left( \beta_0^{-1} (\hat{\mathbf{\Psi}}^{(l)})^T \hat{\mathbf{\Psi}}^{(l)} + \mathbf{A}^{-1} \right)^{-1}, \quad (14)$$

$$\hat{\mathbf{\Psi}}^{(l)} = \begin{bmatrix} \text{Re}(\mathbf{\Psi}^{(l)}) & -\text{Im}(\mathbf{\Psi}^{(l)}) \\ \text{Im}(\mathbf{\Psi}^{(l)}) & \text{Re}(\mathbf{\Psi}^{(l)}) \end{bmatrix}, \quad (15)$$

$$\mathbf{A} = \text{diag}(\alpha_1, \dots, \alpha_{N_x N_y}, \alpha_1, \dots, \alpha_{N_x N_y}), \quad (16)$$

and  $\hat{\mathbf{y}}^{(l)} = [\text{Re}(\mathbf{y}^{(l)}), \text{Im}(\mathbf{y}^{(l)})]^T$ .

Given  $\boldsymbol{\alpha}$  and  $\beta_0$ , the mean and covariance of each scattering coefficient can be obtained using (13) and (14). The associated learning problem thus becomes a search for the parameters  $\boldsymbol{\alpha}$  and  $\beta_0$ . A fast learning algorithm of  $\boldsymbol{\alpha}$  was proposed and the updated expression of  $\boldsymbol{\alpha}$  is expressed as in [16],

$$\alpha_p^{(\text{new})} = \sqrt{\frac{1}{\eta} \sum_{k=1}^{2K} \sum_{l=1}^L \left[ \hat{\boldsymbol{\omega}}_{p+(k-1)N_x N_y}^{(l)} \right]^2}, \quad (17)$$

where

$$\eta = \sum_{k=1}^{2K} \sum_{l=1}^L \text{Tr} \left[ \mathbf{C}_l^{-1} \left( \hat{\mathbf{\Psi}}_{p+(k-1)N_x N_y}^{(l)} \right)^T \hat{\mathbf{\Psi}}_{p+(k-1)N_x N_y}^{(l)} \right],$$

$\mathbf{C}_l = \beta_0 \mathbf{I} + \hat{\mathbf{\Psi}}^{(l)} \mathbf{A} (\hat{\mathbf{\Psi}}^{(l)})^T$ , and  $\hat{\mathbf{\Psi}}_p^{(l)}$  is the  $p$ -th in the  $\hat{\mathbf{\Psi}}^{(l)}$ . Also, the noise precision  $\beta_0$  is updated by [14, 16]

$$\beta_0^{(\text{new})} = \frac{\sum_{l=1}^L \left\{ \text{Tr} \left[ \boldsymbol{\Sigma}^{(l)} \hat{\mathbf{\Psi}}^{(l)} (\hat{\mathbf{\Psi}}^{(l)})^T \right] + \left\| \hat{\mathbf{y}}^{(l)} - \hat{\mathbf{\Psi}}^{(l)} \boldsymbol{\mu}^{(l)} \right\|_2^2 \right\}}{2KML}. \quad (18)$$

Note that  $\alpha^{(\text{new})}$  and  $\beta_0^{(\text{new})}$  are functions of  $\{\hat{\omega}^{(l)}\}_{l=1}^L$ ,  $\{\mu^{(l)}\}_{l=1}^L$  and  $\{\Sigma^{(l)}\}_{l=1}^L$ , while  $\{\hat{\omega}^{(l)}\}_{l=1}^L$ ,  $\{\mu^{(l)}\}_{l=1}^L$  and  $\{\Sigma^{(l)}\}_{l=1}^L$  are functions of  $\alpha$  and  $\beta_0$ . This suggests an iterative algorithm, which iterates (12), (13), (14) and (17), (18), until a convergence criterion is satisfied.

#### 4. SIMULATION RESULTS

In the simulations, a 40-element monostatic ULA with an inter-element interval of 2.5 cm is used for imaging. The origin of the coordinate system is chosen to be the center of the array. The front wall is located parallel to the array at 1 m downrange and its effect is ignored due to perfect wall parameter estimation and compensation, as described earlier. We consider three interior walls; the left and right walls are located at  $\pm 2$  m crossrange, while the back wall is at 5 m downrange.

A stepped-frequency signal, consisting of 360 equally spaced frequency steps from 1.5 GHz to 2.5 GHz band, is employed for scene. The entire bandwidth is uniformly divided into 3 subbands. The scattering coefficients are assumed invariant in each subband, whereas they differ across the subbands. The scattering coefficients in the direct path are drawn from  $\mathcal{N}(0, 1)$ , and the amplitudes of reflectivity in the multipath propagations decay with the distance. Only 20% frequencies and 20% array elements in each subband are randomly selected for the CS-based imaging whereas the full data set is used when performing conventional backprojection (BP) algorithm.

In the simulation,  $Q = 8$  scatterers are adopted. As shown in Fig. 2(a), 4 scatterers are clustered together in the center whereas the other 4 scatterers are distantly located. The adjacent interval along both crossrange and downrange is 0.075 m. The received signal comprises of the direct return along with reflected paths via three interior walls, yielding a total number of  $K = 4$  paths. An additive Gaussian noise with a variance of 0.1 is added in the simulated measurements.

The results depicted in Fig. 2(b) and Fig. 2(c) do not utilize the multipath model for image reconstruction. In particular, Fig. 2(b) shows the reconstruction result using conventional BP algorithm [1]. It is observed that the downrange resolution is reduced due to frequency-dependent scattering coefficients that prevent coherently accumulation across all subbands and thus yield defocused images. In addition, we also observe many ghosts in the reconstructed image as a result of multipath propagation, making the image highly cluttered. Fig. 2(c) shows the result based on CMT-BCS algorithm [16] which only considers group sparsity across subbands without assuming the multipath propagation model, resulting in a high number of ghost targets.

The imaging results depicted in the sequel assume the multipath propagation model as well the group sparsity embedded therein. We first perform the proposed MCMT-BCS approach to process the data in each subband separately, and the fused image of all subband images is shown in Fig. 2(d). It is observed that the consideration of the multipath propagation model effectively suppresses the distant ghost targets, while some spurious targets remain due to the narrow frequency bandwidth in each single subband. Fig.

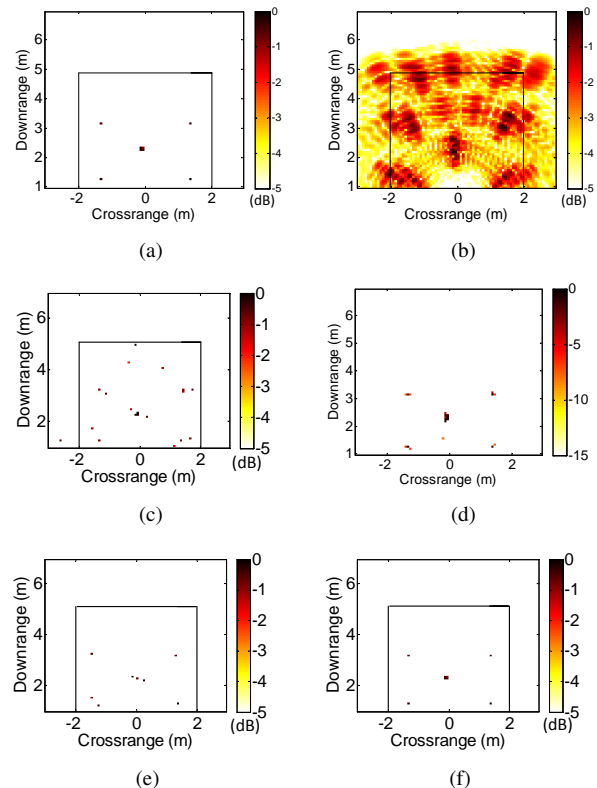


**Fig. 2.** Comparison of reconstruction results. (a) original scene; (b) result of BP; (c) result of CMT-BCS without group sparsity of multipath; (d) fused result of individually constructed images; (e) result of BOMP; (f) result of the proposed algorithm.

2(e) shows the result of the BOMP algorithm that uses all the three subbands with the true sparsity, which fails to acquire the true target positions because of the high coherence in the measurement matrix. Finally, Fig. 2(f) shows the successfully reconstructed result of all targets based on the proposed algorithm that uses all three subbands. In general, the proposed algorithm significantly improves the recovery performance of targets by exploiting group sparsity across multipath propagations and multiple subbands. Note that the proposed technique is capable of automatical inference of the scene sparsity.

#### 5. CONCLUSION

There exists two types of group sparsity in a typical stepped-frequency through-the-wall radar imaging (TWRI) system when multipath propagation is considered and the targets exhibit frequency-dependent scattering characteristics. In this paper, a frequency-dependent subband scattering model is developed to characterize real-world scattering mechanism, and the TWRI is then formulated as the sparse signal recovery problem across all subbands and all paths. A novel modified complex multi-task Bayesian compressive sensing algorithm is proposed to account for these two types of group sparsity and perform high-resolution sparse target imaging in the presence of highly coherent measurement matrix. The proposed algorithm is developed based on the nonparametric hierarchal Bayesian model and, thereby, does not require any prior information of target sparsity.

## REFERENCES

- [1] M. G. Amin, *Through-the-Wall Radar Imaging*. CRC Press, 2010.
- [2] G. Wang, M. G. Amin, and Y. Zhang, "A new approach for target locations in the presence of wall ambiguity," *IEEE Trans. Aerospace Electron. Syst.*, vol. 42, no. 1, pp. 301–315, 2006.
- [3] Y. Zhang, M. G. Amin, and F. Ahmad, "A novel approach for moving multi-target localization using dual frequency radars and time-frequency distributions," in *Proc. Asilomar Conf. Signals, Systems, and Computer*, (Pacific Grove, CA), Nov. 2007.
- [4] F. Ahmad and M. G. Amin, "Multi-location wideband synthetic aperture imaging for urban sensing applications," *J. Franklin Inst.*, vol. 345, no. 6, pp. 618–639, 2008.
- [5] F. Ahmad, Y. Zhang, and M. G. Amin, "Three-dimensional wideband beamforming for imaging through a single wall," *IEEE Geosci. Remote Sens. Lett.*, vol. 5, no. 2, pp. 176–179, 2008.
- [6] M. G. Amin and F. Ahmad, "Wideband synthetic aperture beamforming for through-the-wall imaging," *IEEE Signal Processing Magazine*, vol. 25, no. 4, pp. 110–113, 2008.
- [7] Y. D. Zhang and A. Hunt, "Image and localization of behind-the-wall targets using linear and distributed apertures," in M. G. Amin (Ed.), *Through the Wall Radar Imaging*, CRC Press, 2010.
- [8] S. Kidera, T. Sakamoto, and T. Sato, "Extended imaging algorithm based on aperture synthesis with doublescattered waves for UWB radars," *IEEE Trans. Geosci. Remote Sens.*, vol. 49, no. 12, pp. 5128–5139, 2011.
- [9] P. Setlur, M. Amin, and F. Ahmad, "Multipath model and exploitation in through-the-wall and urban radar sensing," *IEEE Trans. Geosci. Remote Sens.*, vol. 49, no. 10, pp. 4021–4034, 2011.
- [10] M. Leigsnering, F. Ahmad, M. G. Amin, and A. M. Zoubir, "Compressive sensing based specular multipath exploitation for through-the-wall radar imaging," in *Proc. IEEE ICASSP*, (Vancouver, Canada), May 2013.
- [11] L. Jacob, G. Obozinski, and J. Vert, "Group Lasso with overlap and graph Lasso," in *Proc. Int. Conf. on Machine Learning*, (Montreal, Canada), Jun. 2009.
- [12] E. V. D. Berg and M. Friedlander, "Probing the pareto frontier for basis pursuit solutions," *SIAM Journal on Scientific Computing*, vol. 31, no. 2, pp. 890–912, 2008.
- [13] M. Yuan and Y. Lin, "Model selection and estimation in regression with grouped variables," *Journal of the Royal Statistical Society Series B*, vol. 68, no. 1, pp. 49–67, 2006.
- [14] M. E. Tipping, "Sparse Bayesian shrinkage and selection learning and the relevance vector machine," *Journal of Machine Learning Research*, vol. 1, no. 9, pp. 211–244, 2001.
- [15] S. Ji, D. Dunson, and L. Carin, "Multitask compressive sampling," *IEEE Trans. Signal Proc.*, vol. 57, no. 1, pp. 92–106, 2009.
- [16] Q. Wu, Y. D. Zhang, M. G. Amin, and B. Himed, "Complex multitask Bayesian compressive sensing," in *Proc. IEEE ICASSP*, (Florence, Italy), May 2014.
- [17] Y. S. Yoon and M. G. Amin, "Spatial filtering for wall clutter mitigation in through-the-wall radar imaging," *IEEE Trans. Geosci. Remote Sens.*, vol. 47, no. 9, pp. 3192–3208, 2009.
- [18] A. Chandra, D. Gaikwad, D. Singh, and M. Nigam, "An approach to remove the clutter and detect the target for ultra-wideband through-wall imaging," *J. Geophysics and Engineering*, vol. 5, no. 4, pp. 412–419, 2008.
- [19] F. Tivive, A. Bouzerdoum, and M. Amin, "An SVD-based approach for mitigating wall reflections in through-the-wall radar imaging," in *Proc. IEEE Radar Conf.*, (Kansas, MO), Dec. 2011.
- [20] J. Huang and T. Zhang, "The benefit of group sparsity," *Ann. Statist.*, vol. 38, no. 4, pp. 1978–2004, 2010.
- [21] R. G. Baraniuk, "Compressive sampling," *IEEE Signal Process. Mag.*, vol. 24, no. 4, pp. 118–124, 2007.